PERGAMON

Applied Geochemistry 17 (2002) 633–648

Applied Geochemistry

www.elsevier.com/locate/apgeochem

The colloid chemistry of acid rock drainage solution from an abandoned Zn–Pb–Ag mine

Harald Zänker[a,*], Henry Moll[a], Wolfgang Richter[a], Vinzenz Brendler[a], Christoph Hennig[a], Tobias Reich[a], Andreas Kluge[b,1], Gudrun Hüttig[a]

[a]*Forschungszentrum Rossendorf e.V., Institute of Radiochemistry, PO Box 510119, 01314 Dresden, Germany*
[b]*TU Bergakademie Freiberg, Institute of Mineralogy, Brennhausgasse 14, 09596 Freiberg, Germany*

Received 25 January 2001; accepted 17 September 2001
Editorial handling by O. Selinus

Abstract

Acid rock drainage (ARD) solution from an abandoned ore mine (pH 2.7, SO_4^{2-} concentration 411 mmol/l, Fe concentration 93.5 mmol/l) was investigated by photon correlation spectroscopy, centrifugation, filtration, ultrafiltration, scanning electron microscopy, ICP–MS, AAS, ion chromatography, TOC analysis, and extended X-ray absorption fine structure (EXAFS) spectroscopy. A colloid concentration of $\geqslant 1$ g/l was found. The prevailing particle size was <5 nm. Iron, As and Pb were the metal constituents of the colloidal particles. The most probable mineralogical composition of the particles is a mixture of hydronium jarosite and schwertmannite. A small amount of a relatively coarse precipitate was formed in the ARD solution during the months after sampling. The colloid particles are obviously an intermediate in the precipitate formation process. The results suggest that the arsenate is bound to the colloids by the formation of a bidentate binuclear inner-sphere surface complex. However, the transformation of the colloidal material to the more aggregated long-term precipitate results in the incorporation of the arsenate into the interior of the Fe hydroxy sulfate crystal structures. Lead seems to occur as anglesite.

1. Introduction

Gangues of clay minerals that are impregnated with finely-divided sulfide ores play a key role in the sulfide oxidation process in abandoned ore mines. Highly mineralized, red-colored solutions are formed in the pores of these gangues. They result in acid rock drainage (ARD) which can be extremely acidic (see, for instance, Nordstrom et al., 2000). The access of ARD solutions to the bulk waters of a mine is a major factor influencing the composition of mining effluents (Winland et al., 1991; Bigham et al.; 1996; Geller et al.; 1996; Balistrieri et al., 1999; Paulson and Balistrieri, 1999). In the Freiberg (Germany) mining area pore waters from sulfide-rich clay mineral gangues with pH values of 0.7–2.5 have been observed (Haubrich et al., 1999). There is general lack of knowledge as to the chemical speciation of the constituents of such ARD solutions. In particular the colloid-chemistry of such waters has scarcely been studied. However, colloids can significantly influence the properties of ARD solutions. They can play an important role in the transfer of truly dissolved heavy metals into precipitates and can also form aqueous species of permanent stability (Charlet and Manceau, 1993; Cornell and Schwertmann, 1996; Schwertmann et al., 1999). Colloids/particles can influence the mobility (Winland et al., 1991) and the bioavailability (Davis et al., 1997; Wang and Guo, 2000) of heavy metals in the environment. The authors investigated samples from an ARD pool in front of a clay gangue in the abandoned 'Himmelfahrt Fundgrube' mine at Freiberg by colloid-chemical methods. This mine used to be a Zn-Pb-Ag mine; it was closed in 1969; the most important ore minerals mined were

* Corresponding author. Tel.: +49-351-260-3209; fax: +49-351-260-3553.
E-mail address: h.zaenker@fz-rossendorf.de (H. Zänker).
[1] Present address: TU Bergakademie Freiberg, Universitätsrechenzentrum, Bernhard-von-Cotta-Straβe 1, D-09596 Freiberg, Germany.

0883-2927/02/$ - see front matter
PII: S0883-2927(01)00126-3

sphalerite, galena, pyrite, chalcopyrite, and (in the Middle Ages) native Ag. Important gangue minerals are calcite, fluorite, baryte, siderite, and quartz. For details concerning the 'Himmelfahrt Fundgrube' mine see Bayer (1998). The pH of the ARD solution investigated was 2.7, the SO_4^{2-} concentration was 411 mmol/l. The goal was to find out if colloidal particles play a role in the chemistry of the ARD solution under study. Colloidal particles are defined as particles of the size range from 1 nm to 1 μm. They can clearly be distinguished from the smallest units of solutions of truly dissolved heavy metals, the heavy metal ions. The moieties lying between ion size and colloid size, sometimes addressed as clusters, polymers, aggregates etc., shall also be called 'particles' (but not necessarily 'colloidal particles') here. First, the authors wanted to determine the concentration, the size and the chemical composition of the colloids detectable. Second, an attempt was made to analyze the mineralogy of the colloidal particles that were found. Third, it was intended to characterize the type of binding of trace elements such as As onto the colloidal particles.

2. Experimental

2.1. Sampling and on-site analyses

ARD water samples were taken by scooping from an open ARD pool in front of a clay gangue. The samples were of reddish color but visibly clear. The sample temperature, the pH, the redox potential, the O_2 concentration, and the conductivity were determined on-site with the aid of a portable 'Multi Line F/SET' type multiparameter measuring device (WTW GmbH, Weilheim, Germany). The device had been calibrated the same day, before entering the mine. Furthermore, a 10-ml aliquot of the solution was filtered through a 5-μm syringe filter (Minisart, Sartorius AG, Göttingen, Germany) and a 10-ml aliquot through a 450-nm syringe filter (type Minisart). The filtrates of these filtrations were acidified with concentrated HNO_3 at the sampling site for analysis by inductively coupled plasma mass spectrometry (ICP–MS) and atomic absorption spectrometry (AAS) at Rossendorf. All samples were stored and transported in polyethylene vessels that had been cleaned with 1M HNO_3 and rinsed with Milli-Q water (Millipore, Eschborn, Germany). The colloid investigations began about 3 h after sampling.

2.2. Analytical methods

First, the samples were investigated with respect to particle size distribution by photon correlation spectroscopy (PCS). A BI-90 instrument (Brookhaven Instruments Corp., Holtsville, USA) was used which works at a fixed angle of 90°. An Ar ion laser operated at a wavelength of 514.5 nm and at a laser power of 400 mW (LEXEL Laser, Inc., Fremont, USA) served as the light source. Rectangular SUPRASIL cuvettes (Hellma GmbH, Müllheim, Germany) that emit very little scattered light were used. The temperature of the solution was 25 °C, and the duration of the measurements was chosen between 60 and 300 s. The primary information obtained by a PCS measurement is the autocorrelation function $C(\tau)$ of the scattered light intensity fluctuations which is defined by (cf. Weiner, 1984; Ford, 1985):

$$C(\tau) = \lim_{N\to\infty} \frac{1}{N}\sum_{j=1}^{N} n_j n_{j-m}, \quad m = 1, 2, 3, \ldots M \qquad (1)$$

where

$C(\tau)$ = autocorrelation function
n = number of pulses registered during the sampling time $\Delta t = t - \tau$,
with
t = time, $t = j\Delta t$,
τ = delay time, $\tau = m\Delta t$,
Δt = time increment into which the time axis has been divided (sampling time),
N = total number of samples $T / \Delta t$,
with
T = measuring time,
M = number of correlator channels,
j, m = running terms.

For deriving the particle size distributions from the measured autocorrelation functions the non-negatively constrained least squares (NNLS) deconvolution (Grabowski and Morrison, 1983) and the CONTIN deconvolution (Provencher, 1982) were used.

Further methods to characterize the colloidal particles were filtration (Nuclepore polycarbonate filters, Costar, Cambridge, USA), ultrafiltration with YM membranes ('Centriprep', 'Centriplus' and stirred ultrafiltration cell 'Model 8200' from Amicon, Beverly, USA), centrifugation (Kontron T 124, Kontron GmbH, Neufahrn, Germany) and scanning electron microscopy with energy-dispersive X-ray analysis, SEM/EDX (Zeiss, Oberkochen, Germany). The centrifugates, filtrates and particles on the filters were analyzed by ICP–MS (Elan 5000, Perkin Elmer, Überlingen, Germany) and/or AAS (AAS 4100, Perkin Elmer, Überlingen, Germany). Blank values of the experiments and detection limits of the metal analyses were in the range of ng/l, i.e. far below the concentration of the metals of interest (exception: K). Further analytical methods were ion chromatography, IC (Jasco, Groβumstadt, Germany), and total organic C (TOC) analysis (Analysator Multi NC, Analytik Jena GmbH, Jena, Germany). The Fe(II)/Fe(III) ratio of the solutions was determined with 1,10 phenanthroline according to DIN 38406 (1983). X-ray

diffraction was carried out with an URD 6 type X-ray diffractometer (Freiberger Präzisionsmechanik, Freiberg, Germany) using Cu K_α radiation.

Extended X-ray absorption fine structure (EXAFS) measurements on sample fractions and on model substances were performed. The ARD solutions were filtered through filters of different pore sizes (5 μm, 1 kD) after 10 months of equilibration at 5 °C in darkness. The obtained sample fractions were transferred into polyethylene cuvettes of 3 mm diameter to measure Fe K-edge X-ray absorption spectra. For the As K-edge measurements the path length was 13 mm. Schwertmannite (ideally $Fe_8O_8(OH)_6SO_4$) was prepared as described by Arnold et al. (1999). A quantity of 7.26 g K_2SO_4 was dissolved in 3 l of Milli-Q water. Then the solution was heated to 60 °C in a water bath. While steadily stirring the solution, 16.16 g of $Fe(NO_3)_2x9H_2O$ was added. This mixture was left standing for an additional 12 min. Then the schwertmannite suspension was transferred into dialysis tubes and dialyzed until the conductivity of the surrounding liquid was practically that of pure water. The minerals scorodite ($FeAsO_4{\cdot}2H_2O$) and bukowskyite ($Fe_2AsO_4SO_4OH{\cdot}7H_2O$) came from Dr. F. Krantz Rheinisches Mineralien-Kontor. Jarosite ($KFe_3(SO_4)_2(OH)_6$) was precipitated from an acidic Fe(II) sulfate solution containing K^+ and *Thiobacillus ferrooxidans* cells. The goethite (α-FeOOH) sample was synthesized according to Cornell and Schwertmann (1996). All model substances were analyzed using XRD and/or SEM/EDX. The solid samples used to measure the EXAFS spectra from the model compounds were prepared by mixing appropriate amounts of the solid with teflone and then pressing to give pellets with a diameter of 13 mm. The measurements gave an edge jump of ~1.0 across the Fe and As K absorption edge.

The EXAFS data were recorded at the Rossendorf Beamline (ROBL) at the ESRF in Grenoble. For details concerning this beamline see Matz et al. (1999). Transmission and/or fluorescence spectra were measured at room temperature using a cooled Si(111) double-crystal monochromator of fixed-exit type ($E = 5$–35 keV). Higher harmonics were rejected using two Si and Pt coated mirrors; the Si coated part of the mirror was used for the Fe K-edge, the Pt coated part for the As K-edge. For energy calibration of the sample spectra, the spectrum from a Fe or Pt foil was recorded simultaneously. The ionization energy of the Fe and As K-edge, E_0, was arbitrarily defined as 7 132 and 11 825 eV. The data were treated using the EXAFSPAK software developed by George and Pickering (1995). Theoretical backscattering phase and amplitude functions, $\delta(k)$ and $F(k)$, used in data analysis, were calculated using the FEFF7 (Zabinsky et al., 1995) program. The EXAFS oscillations, $\chi(k)*k^3$, were isolated using standard procedures for pre-edge subtraction, spline removal, and data normalization (Koningsberger and Prins, 1988).

3. Results and discussion

3.1. Chemical analysis

Table 1 gives the data of the on-site analyses and Table 2 gives the ICP–MS, AAS and IC results. Two

Table 1
On-site field parameters from the sampled ARD pool (unfiltered solution)

Temperature (°C)	8.2±0.1
pH	2.7±0.1
Redox potential E_H (mV)	670±10
Oxygen concentration (mg/l)	0.90±0.03
Electrical conductivity (mS/cm)	14.2±0.2

Table 2
Chemical analysis of the ARD solution by ICP–MS, IC and/or AAS (unfiltered sample). Two measuring series each including 7 measurements were taken

Component	Concentration (mmol/l)			
	Measuring series 1		Measuring series 2	
	Mean	Standard deviation	Mean	Standard deviation
Al[b]	49.8	0.6	54.4	0.4
As[c]	6.29	0.06	6.73	0.09
Ca[c]	12.43	0.18	10.43	0.55
Cd[b]	0.266	0.004	0.26	0.01
Ce[b]	0.046	0.001	0.048	0.002
Co[b]	0.11	0.02	0.091	0.004
Cr[b]	0.062	0.001	0.061	0.001
Cu[b]	1.52	0.02	1.58	0.01
Fe[c]	82.2	1.1	94.3	2.0
K[d]	nd[a]	–	nd	–
La[b]	0.014	0.001	nd	–
Li[b]	0.48	0.01	0.50	0.03
Mg[b]	86.1	0.9	93.7	0.5
Mn[b]	22.7	0.2	25.2	0.1
Na[d]	nd	–	nd	–
Ni[b]	0.21	0.03	0.19	0.01
Pb[b]	0.11	0.03	0.09	0.02
Si[b]	2.52	0.04	2.75	0.01
Th[b]	0.0076	0.0001	0.0074	0.0004
U[b]	0.0075	0.0001	0.0076	0.0004
Y[b]	0.063	0.001	0.060	0.003
Zn[b]	75.1	0.9	82.2	0.5
Sulfate[e]	409	14	411	14
Chloride[e]	nd	–	nd	–
Nitrate[e]	nd	–	nd	–

[a] nd—Not detectable.
[b] ICP–MS.
[c] ICP–MS, AAS.
[d] AAS.
[e] IC.

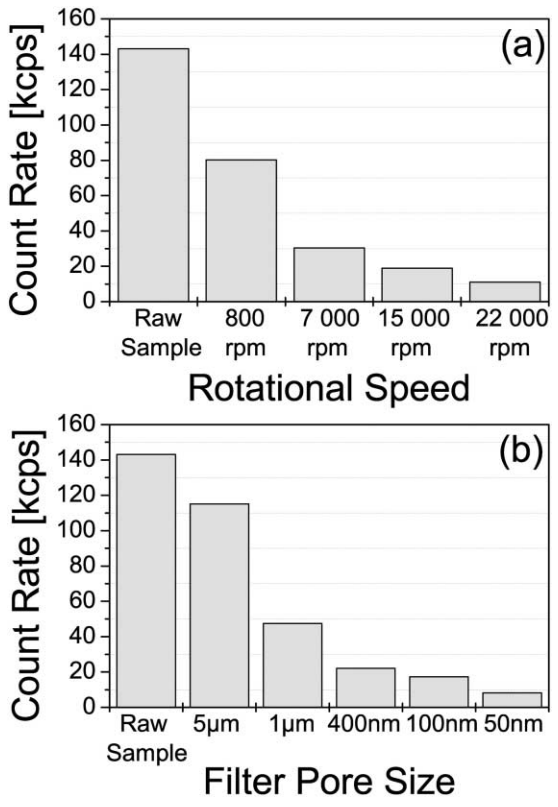

Fig. 1. Scattered light intensity (count rate of the photomultiplier) after (a) 1-hour centrifugation at different rotational speed and (b) filtration through Nuclepore filters of decreasing pore size. Whereas the chemical concentrations do not decrease by centrifugation or filtration (not given here), the scattered light intensity does.

ICP–MS measuring series each including 7 measurements were taken. The experimental scattering within each of these data series is very small as the standard deviations in columns 3 and 5 of Table 2 show. However, for some elements there is a slight systematic deviation between the value in series 1 and the value in series 2 the reason of which is unclear (it should be associated with the complex matrix of the ARD samples). The difference does in no case exceed 15% and it does not have significant influence on the geochemical conclusions drawn from these data (speciation modeling by EQ3/6; cf. 3.3.1.). The TOC concentration was 19.3 mg/l. One day after sampling, 9% of the Fe was identified as Fe (II). On the eleventh day, this value had decreased to 0.5%.

Thus the ARD samples can be characterized as a relatively concentrated acidic SO_4^{2-} solution with an O_2 content that is worth mentioning. The redox potential is obviously not in equilibrium with O_2 which is not surprising for a natural water (cf. Lindberg and Runnells, 1984). The Fe is partly divalent. The major cationic components are Zn, Fe, Mg, Al, and Mn. Important minor components are As, Cu, Pb and Cd. The TOC content is noticeable.

3.2. Colloid inventories

3.2.1. PCS on the raw sample

The scattered light intensity of the ARD solution was by a factor of 50 higher than that of the extremely particle-free Milli-Q water (Milli-Q water purification system with ultrafilter and UV irradiation unit), indicating the presence of particles. PCS on the raw sample revealed a prevalent particle size of about 100 nm. Filtration through a 5-µm Nuclepore filter to improve the counting statistics by removing possible large scatterers did not significantly change the PCS result. For autocorrelation functions and PCS particle size distributions see Section 3.2.2. where PCS is combined with colloid fractionation techniques making PCS particularly powerful.

3.2.2. Centrifugation and filtration

Parallel centrifugation of sample aliquotes were performed (i.e. of a series of subsamples of the original water) with increasing centrifugal force and parallel filtration of aliquotes (subsamples of the original water again) with Nuclepore filters of decreasing pore size in a similar way to that described by Zänker et al. (2000). The highest centrifugal acceleration was $40{,}000\times\ g$ (centrifugation time 1 h) which corresponds to a maximum size of the particles still present in the centrifugate of about 10 nm. The smallest Nuclepore filter size was 50 nm.

In contrast to the authors results on an adit water (Zänker et al., 2000), none of the chemical elements showed a significant response to the filtrations (both the filtrations carried out at the sampling site and in the laboratory) and the centrifugations. Quite different was the behavior of the scattered light intensity which dropped strongly, indicating the removal of particles by the sample treatment (Fig. 1). Nevertheless, even the centrifugates/filtrates of the most rigorous treatment still showed a scattered light intensity which was by a factor of about 5 higher than that of Milli-Q water. PCS was possible on all the centrifugates and filtrates. It revealed that the above-mentioned 100-nm particles form only the minor colloid component. Fig. 2 shows the autocorrelation functions [cf. Eq. (1)] of several sample fractions. The autocorrelation functions contain information on the time-dependent relaxation of concentration fluctuations in a solution. In the present case, these fluctuations are primarily caused by the translational diffusion of rigid particles. Monodisperse spherical particles of 10 nm, for instance, reach practically full relaxation (decay of the autocorrelation function to the baseline) after about 10^2 µs. The autocorrelation function of a polydisperse real sample is the sum of different decaying contributions, normally

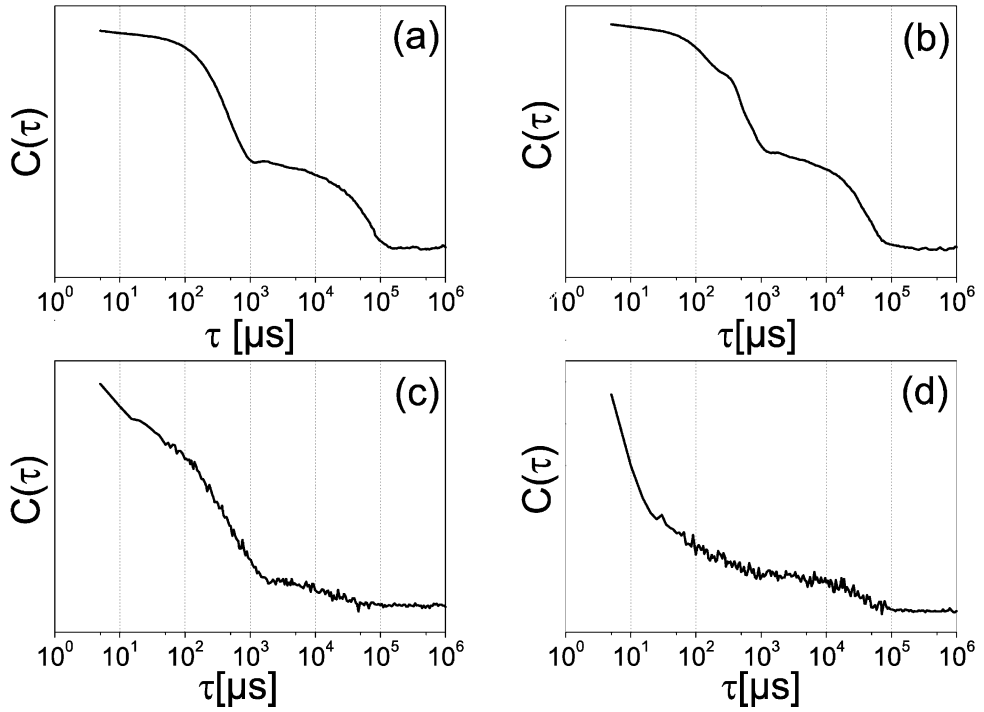

Fig. 2. Autocorrelation functions of the light scattered from the ARD sample: (a) raw sample, (b) 5-μm filtrate, (c) 400-nm filtrate, (d) 50-nm filtrate. Laser power 400 mW. First delay time 5 μs. Last delay time 1 s. Measuring time 120 s.

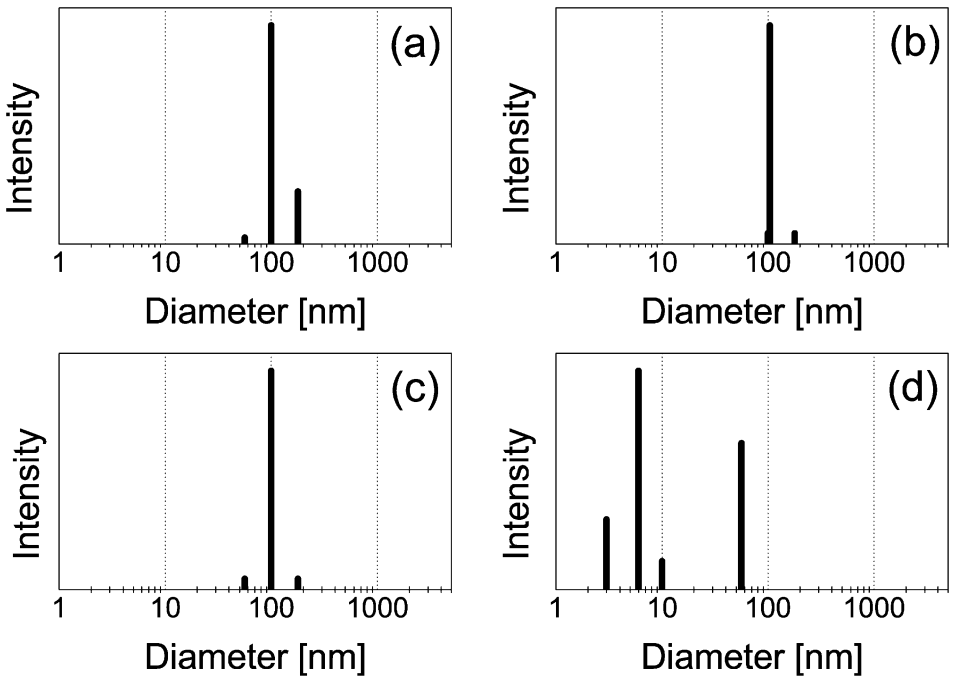

Fig. 3. Light-intensity weighted particle size distribution in the ARD sample according to the CONTIN deconvolution of the autocorrelation functions. (a) Raw sample, (b) 5-μm filtrate, (c) 400-nm filtrate, (d) 50-nm filtrate. Removing the larger submicron particles results in the appearance of the weakly scattering ultrafine particles (< 10 nm) as shown in (d).

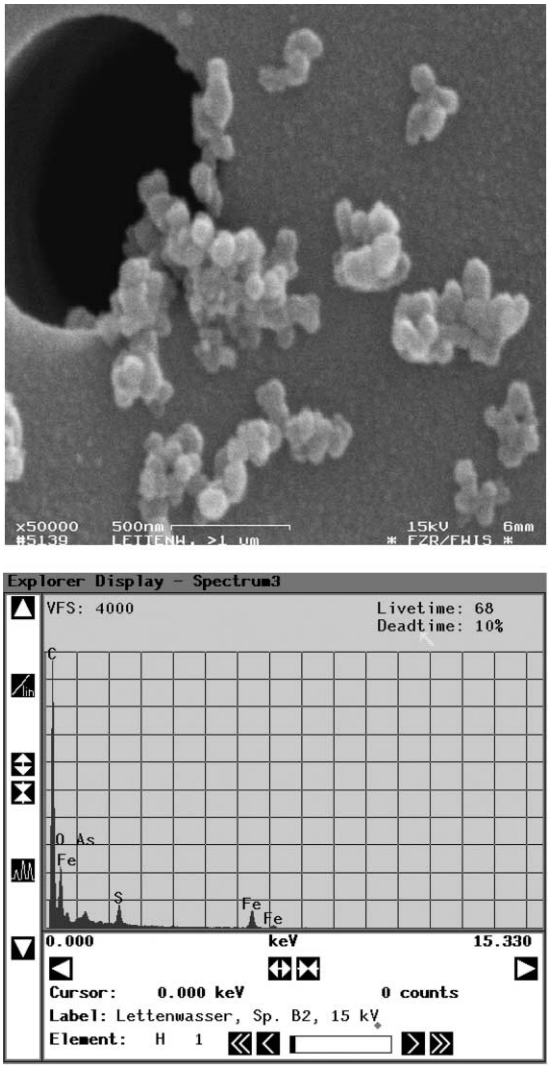

Fig. 4. SEM micrograph (coating with Au) and EDX spectrum (coating with C) of particles on a 1-µm Nuclepore filter. Filter washed three times with Milli-Q water. Particles of about 100 nm are visible. They form aggregates on the filter membrane which probably result from the filtration process and do not exist in solution. Fe, As and S are the main constituents of the particles. The high C peak in the EDX spectrum is caused by the filter material and thus an artifact.

the sum of exponentials (Grabowski and Morrison, 1983; Stock and Ray, 1985; Schurtenberger and Newman, 1993). As one can see, the first 3 autocorrelation functions in Fig. 2 consist primarily of components of relaxation times larger than 10^2 µs. However, the autocorrelation function in Fig. 2d (50-nm filtrate) is different from the others. It shows its major decay already before 10^2 µs. These features of the scattered light fluctuations are also reflected in the CONTIN and the NNLS deconvolutions of the autocorrelation functions (particle size distributions). Fig. 3 demonstrates this for CONTIN. The figure shows that the raw sample and the first two filtrates are dominated by particles of about 100 nm whereas most of the larger submicron particles have been removed by the 50-nm filtration which makes the ultrafine particles of <10 nm detectable by PCS (the detection of extremely small colloid particles can be prevented in the presence of larger submicron particles due to optical masking which results from the r^6 dependence of the scattered light intensity on the particle radius r in the particle size range of Rayleigh scattering). Similar results were obtained by the centrifugation experiments. In this case the ultrafine particles appeared in the PCS spectra after a 1 hr centrifugation at $\geqslant 15\,000 \times g$.

ICP–MS/AAS on the retentates on the 50-nm filters revealed that the strongly-scattering 100-nm particles are a trace component of about 20 mg/l consisting primarily of Fe and As compounds. Fig. 4 shows an SEM micrograph of these 100-nm particles when lying on a Nuclepore filter as well as an EDX spectrum of such particles. The particles are arranged on the filter as aggregates of about 1 µm in diameter. Because of the known susceptibility of filtration to artefacts, it cannot be decided from the SEM images alone whether or not these aggregates exist also in solution. However, it follows from the in-situ measurements by PCS that the 100-nm particles move freely in the solution and that the aggregates are formed on the filter membrane during filtration ('self-coagulation', cf. Buffle and Leppard, 1995). According to EDX, As, Fe and S compounds are the major constituents of these particles. SEM occasionally also revealed the presence of threadlike particels of several microns in length which did not contain heavy metals and seemed to be biogenic, i.e. microorganisms (the TOC concentration filterable by a 50-nm filter was 5 mg/l). The particle population of $\leqslant 10$ nm cannot be visualized by SEM because their size is below the resolution limit of this technique.

3.2.3. Ultrafiltration

The ultrafine particles were investigated more thoroughly by ultrafiltration. The results for 10 selected chemical elements are depicted in Fig. 5. As one can see, decreasing amounts of the elements pass through the filters with decreasing molecular weight cutoff. The sums of the filtrate and the retentate concentrations (the latter were normalized to the original volumes) demonstrate that the filtration recoveries are reasonable: the sums of the ultrafiltration fractions are quite well in agreement with the concentrations of the raw sample (first columns in Fig. 5). Table 3 gives the percentage retention of the most important chemical elements at the 3-kD ultrafilter. Most of the elements show retentions between 7.5 and 13.2%. This group includes elements such as Li, Mg, Cu or Zn which are typically

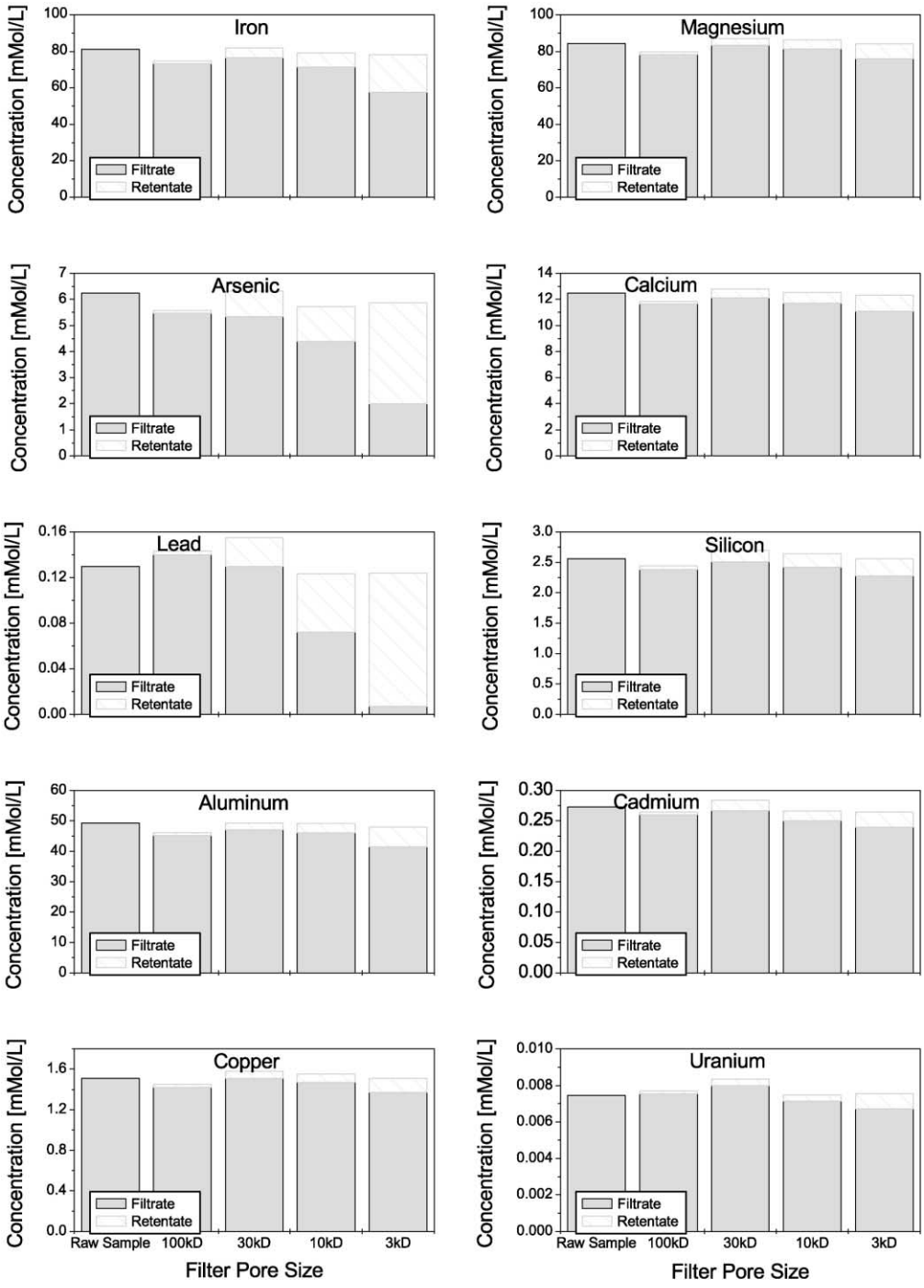

Fig. 5. Concentration of some typical elements in the ultrafiltration fractions (ICP–MS, AAS). The geometric pore size of the 100, 30, 10 and 3 kD filters is about 5, 2, 1.8 and 1.3 nm, respectively. Fe, As and Pb form the colloidal component of the ARD sample (S was not analyzed).

ionogenic in acidic SO_4^{2-} solutions (compare also the results by Pleβow and Heinrichs, 2000). It is supposed that the retention of these elements is not due to particle filtration. Reverse osmosis may be the reason for this 'nonparticulate' retention. However, 3 chemical elements fall unambiguously outside this group: Fe, As, and Pb. If the retentate concentrations of these 3 elements are compared with the raw sample value (first columns in Fig. 5), a rough estimation of the amount of colloidal particles present in the ARD solution can also

Table 3
Retention of selected chemical elements by the 3 kD (about 1.3 nm) ultrafilter

Element	Retention (%)
Al	13.2
As	62.0
Ca	9.7
Cd	9.1
Cu	9.5
Fe	25.4
Li	7.5
Mg	9.5
Mn	9.5
Pb	90.2
Si	10.1
Zn	9.3

be obtained. Assuming that the 'nonparticulate retention' is about 10%, from the retentate-to-raw-sample concentration ratios in Fig. 5 it can be calculated that at least 15% of the Fe, 50% of the As and 80% of the Pb occur as particles of 1.3–5 nm in diameter (the geometric sizes of the 3-kD and the 100-kD filter pores, respectively). They correspond to a colloid concentration of at least 680 mg/l Fe, 230 mg/l As and 20 mg/l Pb in the fresh ARD sample (based on the data in Fig. 5 again). No information can be obtained from these ultrafiltration experiments about particles of the size range between ion size and 1.3 nm. However, it is plausible to expect also particles in this size region. The 1-kD ultrafiltration (cf. Section 3.3.3.) which leads to significantly higher enrichment factors was not included in Fig. 5 because it was carried out 10 months later and was thus not fully comparable with the other ultrafiltrations.

3.3. Colloid mineralogy

3.3.1. Model predictions

The EQ3/6 geochemical speciation software (Wolery, 1992) was used to identify the chemical compounds that are potential colloid-forming compounds. Modeling was performed with unfiltered sample concentrations (Table 2), therefore oversaturation and consequently mineral precipitation is indicated, depending on the various data scenarios that follow. Assumptions are that the colloid concentration is small in the particle size range between ion size and 1.3 nm, and that the sample is not far from thermodynamic equilibrium. All thermodynamic constants are taken from the 'COM' database accompanying EQ3/6, assuming the solubility of colloidal particles being equal to that of macroscopic phases. However, several extensions to the database proved to be necessary, including the addition of solid phases such as ferrihydrite ($Fe_5OH_8{\cdot}4H_2O$), hydronium jarosite ($HFe_3(SO_4)_2(OH)_6$), schwertmannite, and scorodite (Cornell and Schwertmann, 1996; Robins, 1987; Bigham et al., 1996). Because the Na and K concentrations were below detection limit, Na and K values for Freiberg ARD samples from another source (Haubrich et al., 1999) were used.

EQ3NR computations revealed oversaturation of the minerals anglesite ($PbSO_4$), various SiO_2 modifications, Fe minerals such as schwertmannite, jarosite, ferrihydrite, hematite and goethite.

In a second step, EQ3/6 computations took mineral precipitations into account. The modeled nearly complete precipitation of Pb as anglesite was in good agreement with the findings for the colloid compositions (a consideration of plumbojarosite is not possible due to a lack of reliable thermodynamic data). With regard to Si, equilibrium with amorphous silica was indicated. This makes sense because the formation of thermodynamically more stable SiO_2 phases is often kinetically hindered, as has already been found for other natural waters (Iler, 1979). Finally, with regard to the Fe speciation, several scenarios had to be considered to account for uncertainties in phase composition and precipitation kinetics. This also influences the As speciation through Fe arsenates and aqueous Fe/As complexes. Common to all models is the assumption of an oxidizing environment, open to the air, as found in the natural environment of the water samples.

Scenario 1: Only ferrihydrite (log $K_{sol} = 3.0$), schwertmannite, jarosite and Na-jarosite ($NaFe_3(SO_4)_2(OH)_6$) are allowed to precipitate.

Scenario 2: As scenario 1; log K_{sol} for ferrihydrite is assumed to be 5.0 in order to be consistent with Bigham et al. (1996) and their schwertmannite data.

Scenario 3: In addition to scenario 2, H-jarosite ($HFe_3(SO_4)_2(OH)_6$) is allowed to precipitate.

Scenario 4: In addition to scenario 3, scorodite is allowed to precipitate.

Moreover, there are ranges of solubility products, log K_{sol}, of schwertmannite and jarosite given in the literature. The differences for schwertmannite are only reflected in scenario 2a with log $K_{sol} = 20.5$ and 2b with log $K_{sol} = 15.5$ (cf. Bigham et al, 1996), in all the other models no schwertmannite precipitation is predicted. And the two extremes in log K_{sol} for jarosite (ranging from −12.5 to −9.21, cf. Bigham et al., 1996) change the Fe speciation only slightly, with the higher value resulting in the formation of about 0.5% additional jarosite at the maximum. The Fe speciation for the scenarios as discussed above was calculated for both measuring series of element concentrations in Table 2. No significant differences were found for the two measuring series. The results for measuring series 2 are shown in Fig. 6.

The speciation of the truly dissolved Fe fraction is dominated by only three species: $FeSO_4(aq)$ with mole fractions between 42 and 55%, Fe^{2+} (between 28 and 42%), Fe^{3+} (between 2 and 16%). This means that most of the dissolved Fe is present in the reduced form. The

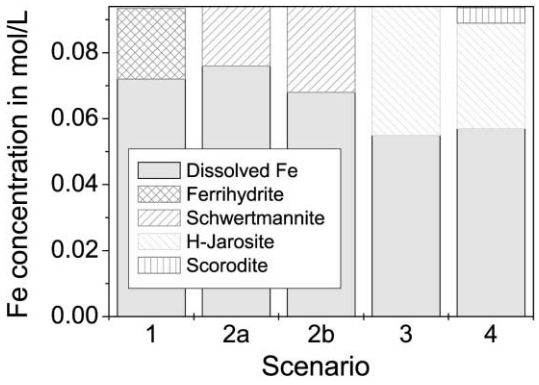

Fig. 6. Fe (total 0.0943 M) distribution in the ARD solution computed with EQ3/6. Chemical composition as given in Table 2, measuring series 2. Description of the scenarios in the text (Section 3.3.1.).

sum of all aqueous Fe–As-complexes does not exceed 4%. These general speciation patterns for the truly dissolved Fe are independent of the considered model scenario. The relatively high proportion of divalent Fe agrees only poorly with the experimental findings (cf. Section 3.1.) which, however, were not in situ results.

The modeling correctly reflected the steadily drifting of the pH from the measured pH 2.7 of the fresh solution to a value of 2.4 after several months. The models predict a final equilibrium pH between 2.05 and 2.25. The redox potential, E_h, is predicted to be between +620 and +690 mV, close to the experimental value of 670 mV.

3.3.2. Information from XRD and EDX (long-term precipitate)

The ARD sample was not in full thermodynamic equilibrium. This can be concluded from the pH drift, from a decrease in the Fe, As, and Pb concentrations during the time after sampling and from the formation of a relatively small amount (< 1g/l) of a coarse precipitate during the months after sampling. The authors were interested in the processes proceeding in the ARD solution after sampling, in particular in the nature of the precipitated solid. The coarse precipitate need not possess the same mineralogical composition as the ultrafine particles under study here. However, there might be a relationship between the two types of solid phases. If so, the mineralogy of the precipitate can possibly give clues concerning the mineralogy of the ultrafine colloid particles.

The metal contents of the precipitate are given in Table 4. The following secondary minerals come into question as the constituents of the solid: scorodite, jarosite, H-jarosite, schwertmannite, ferrihydrite, anglesite ($PbSO_4$), and plumbojarosite ($Pb[Fe_3(SO_4)_2(OH)_6]$). Scorodite cannot have bound more than 1/5 of the Fe because the theoretical molar Fe/As ratio of scorodite is

Table 4
Metal composition of the precipitate that evolved in the ARD sample within 10 months

Component	Concentration (mmol/g)
As	1.1
Fe	5.8
K	0.1
Pb	0.071

1, much less than what was found experimentally. Thus, most of the Fe must be bound as one of the other Fe minerals between which cannot be further differentiated from the results of Table 4. By EDX on the precipitate a molar Fe/S ratio of 3.6 was measured. The expected molar Fe/S ratio is 1.5 for jarosite and 4.6–8.0 for schwertmannite. Therefore, the SO_4-rich mineral jarosite should be the prevailing constituent of the precipitate. This jarosite should be primarily H-jarosite since the content of K is too low to explain the presence of larger amounts of common jarosite. The As may be bound as scorodite or adsorbed (surface complexation). The small amount of Pb may be in the form of anglesite.

The XRD analyses on the solid (Fig. 7) clearly showed that jarosite of the general formula $(K, H_3O)Fe(SO_4)_2(OH)_6$ is the major component of the long-term precipitate. Because of the deficiency in K, this jarosite should be classified as H-jarosite. Scorodite was not detected. However, the presence of a certain amount of poorly crystalline phases (as e.g. schwertmannite) cannot be excluded from the XRD results on the long-term precipitate. As expected no Pb minerals could be observed due to the low Pb content.

3.3.3. Information from EXAFS (colloids and long-term precipitate)

Proceeding from the assumption that there may be a relationship between the long-term precipitate and the ultrafine particles, the authors endeavored to characterize the colloidal particles' mineralogy itself. XRD fails with the ultrafine particles because these particles appear 'amorphous' to XRD. The method of choice for gaining information on the short-range order of 'amorphous' colloids is X-ray absorption spectroscopy (XAS) which provides structural information on the first 2–3 atomic shells surrounding an X-ray absorbing atom. XAS can be employed as a noninvasive in situ method, i.e. the colloidal particles can be studied in their original aqueous environment. However, a problem arises in such in-situ experiments. Colloidal suspensions often are mixtures of particles and truly dissolved species of the same chemical elements between which XAS cannot differentiate. The authors tried to tackle this problem by taking EXAFS spectra at the Fe and As K-edges from

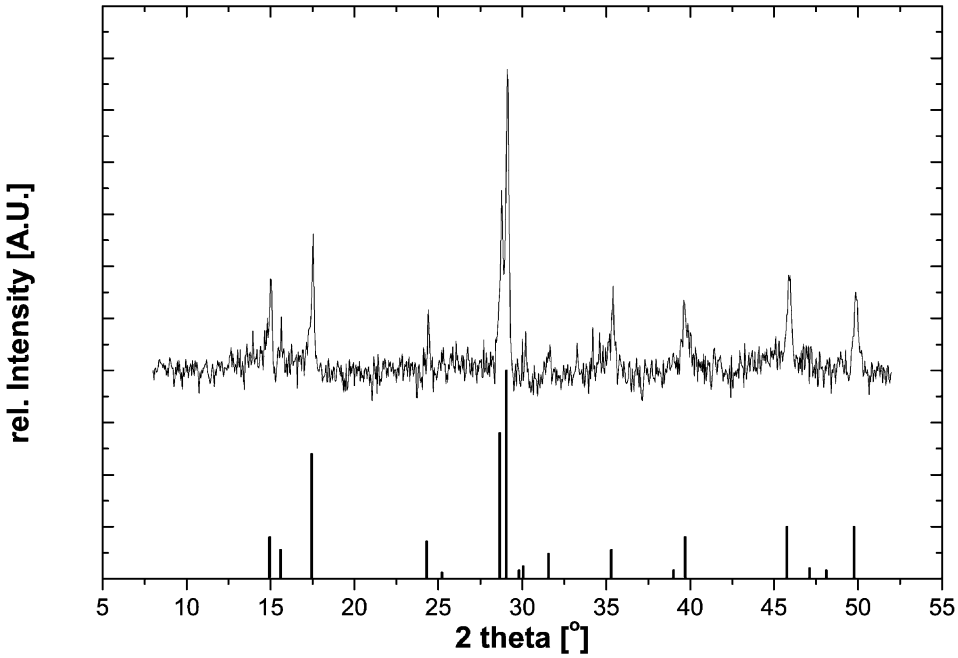

Fig. 7. XRD powder diagram of the precipitate (curve) and the major reflexes of jarosite, $(K,H_3O)Fe_3(SO_4)_2(OH)_6$ (vertical lines) according to Powder Diffraction File (1991).

1. the unfiltered raw samples (and 5-μm filtrates)
2. solutions strongly enriched in colloidal particles (retentates of 1-kD ultrafiltrations)
3. solutions strongly depleted of colloidal particles (filtrates of 1-kD ultrafiltrations).

Furthermore, the long-term precipitate described in Section 3.3.2. was investigated.

The enrichment factor $C_{retentate}/C_{filtrate}$ of the 1-kD (about 1 nm) ultrafiltration was 6.8 for Fe, 58 for As, and 223 for Pb. An important observation was that the scattered light intensity of the 1-kD filtrate gradually rose after the filtration (from 5.6 to 18 kcps within 48 h). The equilibrium of the sample had obviously been disturbed by the ultrafiltration and adjusted itself again by the formation of new particles.

Figs. 8 and 9 show the experimental Fe K-edge and As K-edge EXAFS spectra of several model compounds (schwertmannite, jarosite, goethite, scorodite and bukowskyite) and the ARD sample fractions as well as the corresponding Fourier transforms (FTs). The shown EXAFS oscillations represent a sum parameter consisting of all absorber-backscatterer contributions. Ideally, every peak in the Fourier transform corresponds to a special class of neighboring atoms around the absorbing atom. The determined structural parameters at the Fe K-edge are summarized in Table 5. The EXAFS results for reference compounds show Fe–O bond lengths of 1.96–1.99 Å. This is the typical value for an octahedrally coordinated Fe atom. The edge-shared FeO_6 octahedra in schwertmannite and goethite lead to short Fe–Fe distances of 3.03 Å and 3.37 Å (Table 5). In contrast, the corner-shared FeO_6 octahedra in jarosite result in Fe–Fe distances of 3.66 Å. Fe–As distances in scorodite and bukowskyite are determined by EXAFS analysis as 3.36 Å and 3.34 Å at the Fe K-edge (Fig. 8) and as 3.34 Å and 3.33 Å at the As K-edge (Fig. 9), respectively. The atomic surrounding of Fe in the model compounds jarosite, goethite and scorodite is in fair agreement with XRD data. To the authors knowledge, no EXAFS structure parameters for schwertmannite and bukowskyite have been reported in the literature up to now.

It can be concluded from the similarity between the Fe K-edge EXAFS spectra of the ARD samples that the colloidal particles (unfiltered ARD solution, 1-kD filtrate and 1-kD retentate) and the long-term precipitate have a similar Fe matrix. The Fe-Fe distance of about 3.60 Å indicates a close relationship between the ARD samples and the jarosite. To explore the mineralogy of the colloid particles the authors tried to describe the EXAFS spectra by linear combinations of the EXAFS oscillations of the model compounds. For the long-term precipitate, the best result could be achieved by assuming a mixture of 40% jarosite and 50% schwertmannite. Attempts to describe the EXAFS oscillations of the 1-kD retentate (enriched colloid) gave similar results. This indicates that the colloidal particles seem to be an intermediate in the precipitate formation process having a mineralogy similar to that of the precipitate.

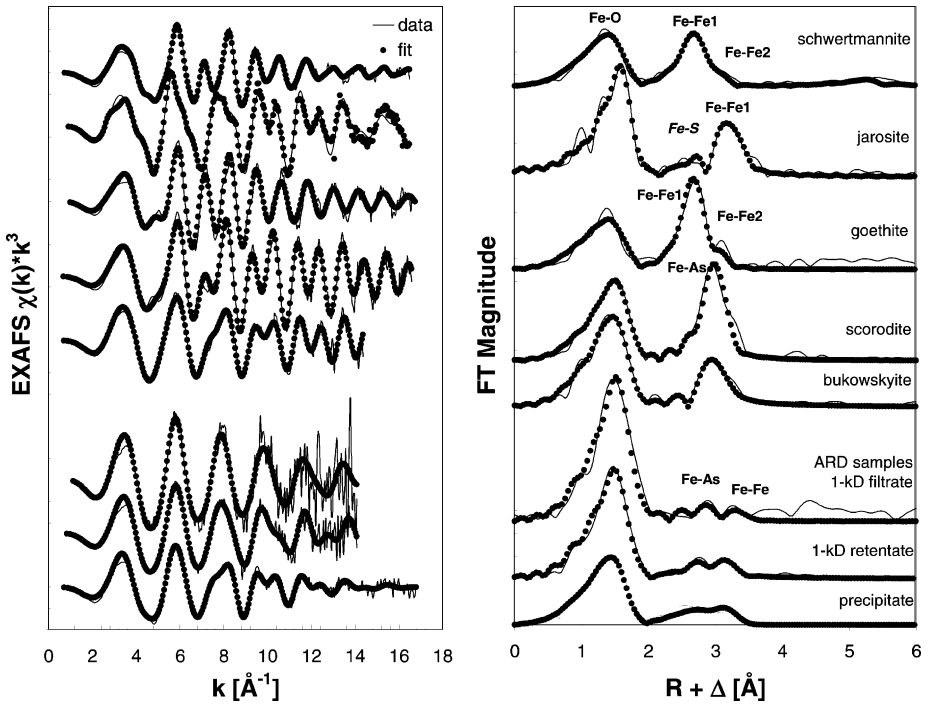

Fig. 8. Fe K-edge k^3-weighted EXAFS spectra (left) and corresponding Fourier Transforms, FTs, (right) of model compounds (schwertmannite, jarosite, goethite, scorodite, bukowskyite) and ARD fractions. The FTs are not corrected for EXAFS phase shifts. The peaks appear at shorter distances ($R + \Delta$) relative to the true near-neighbor distances (R).

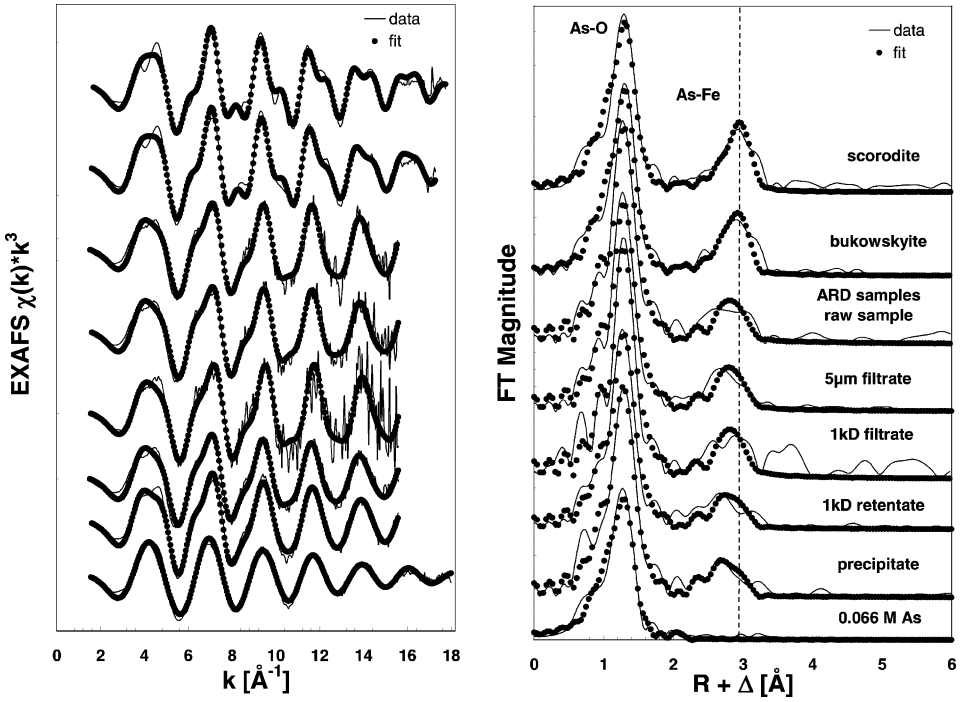

Fig. 9. As K-edge k^3-weighted EXAFS spectra (left) and the corresponding Fourier Transforms, FTs, (right) of model compounds and ARD fractions. The FTs are not corrected for EXAFS phase shifts. The peaks appear at shorter distances ($R + \Delta$) relative to the true near-neighbor distances (R).

The EQ3/6 calculations in Section 3.3.1. predicted either H-jarosite or (if the precipitation of H-jarosite is not allowed) schwertmannite and possibly some scorodite as the probable solid phases. The coexistence of both schwertmannite and H-jarosite in the colloid particles and in the long-term precipitate indicated by the EXAFS spectra shows that the 'solubility window' for schwertmannite of log $K_{sol} = 18.0 \pm 2.5$ given by Bigham et al. (1996) may still be too high. This follows also from measurements by Yu et al. (1999) who found a solubility product of log $K_{sol} = 10.5 \pm 2.5$ for schwertmannite. Thus, in an additional modeling series, the K_{sol} of schwertmannite was systematically varied within this range and indeed a simultaneous precipitation of both schwertmannite and H-jarosite is predicted for schwertmannite K_{sol} values smaller than 8.9. Bigham et al. (1999) separated the solid phase from the 'dissolved' species by using a 200-nm filter which may have caused an overestimation of the schwertmannite solubility. The present colloid-chemical study on an ARD solution demonstrates that a 200-nm filter is an unsatisfactory means for separating the solid and dissolved components of an acidic SO_4^{2-}-rich Fe salt solution. Furthermore, one should consider that even the 1-kD filter (having a geometric pore size of about 1 nm) is not a fully satisfactory means of phase separation. Particles may also exist in the size range below 1 nm. At least for ferrihydrite, there are indications that a structural continuity between ionic species and ferric gels exists (Magini, 1977; Manceau et al., 1992; Charlet and Manceau 1993; Waychunas et al., 1993, 1996; Schwertmann et al., 1999; Byrne and Luo, 2000). Such a continuity should also be supposed for minerals such as schwertmannite and H-jarosite. One should also bear in mind when using the 'solubility windows' from the literature that schwertmannite is a metastable mineral which is gradually transformed into more stable minerals.

It is obvious that the pronounced uncertainties concerning the solubilities of the Fe minerals (solubility 'windows' for ferrihydrite, schwertmannite and jarosite) are a serious obstacle for predicting the Fe behavior in ARD solutions by model calculations. Better thermodynamic (and also kinetic) data are urgently needed for such calculations.

3.4. Bonding of arsenate onto the colloids

3.4.1. Model predictions

The most important toxic contaminant of the colloidal particles in the ARD solution is As (cf. Fig. 5). According to the EQ3/6 calculations, this As should occur in the form of scorodite. However, experimental findings have been published according to which scorodite is stable only at pH values of $\leqslant 2$ (Robins, 1987). This is below the pH of the ARD solution (pH 2.7). Experimental proof of the calculations for As is therefore needed.

3.4.2. Information from EXAFS

Fig. 9 shows the measured $\chi(k)$ spectra and the corresponding FTs obtained from the model compounds, the ARD ultrafiltration fractions 1–3 (cf. section 3.3.3.) and the long-term ARD precipitate measured at the As K-edge. As can be seen, the FTs of the ARD fractions are quite different from that of the pure arsenate solution. They exhibit a pronounced As–Fe contribution at about 3.28 Å (see Fig. 9 and Table 5). On the other hand, the As–Fe distance in the ARD samples is by 0.04–0.08 Å shorter than that of the minerals scorodite and bukowskyite.

The As–Fe distance of 3.28 Å found for all ARD fractions and confirmed also by X-ray absorption near edge structure (XANES) spectroscopy (Moll et al., 2000) can be explained by arsenate uptake by the Fe hydroxy sulfates according to 3 alternative structural mechanisms:

(a) The arsenate may be bound by surface complexation as was reported for the arsenate binding onto ferrihydrite. Waychunas et al. (1993, 1995, 1996) and Fuller et al. (1993) found for this system two different Fe–As distances: 3.28 and 3.60 Å. The short distance is assigned by these authors to a bidentate binuclear (bridging) arsenate surface complex in which the arsenate is attached to O atoms of two iron Fe octahedra. The Fe-As distance of 3.6 Å is assigned to a linear monodentate (corner-sharing) arsenate surface complex. However, the existence of the monodentate complex was disputed by Manceau (1995). According to Manceau (1995), Waychunas et al. (1993) and Fuller et al. (1993) overestimated the Fe–As distance of 3.6 Å by about 0.8 Å due to an error in the fit of the experimental data. The true Fe–As distances are supposed to be 3.28 and 2.8 Å according to Manceau (1995). The distance of 2.8 Å is supposed to represent a bidentate mononuclear (edge-sharing) arsenate surface complex on the ferrihydrite. Fendorf et al. (1997) concluded from EXAFS measurements at the As K-edge on arsenate-contaminated goethite that 3 surface complexes play a role—a monodentate one, a bidentate binuclear one and a bidentate mononuclear one. Whereas there are obviously still arguments about the 2.8 and 3.6 Å distances, agreement seems to exist for the 3.28 Å distance, i.e. the bidentate binuclear surface complex.

(b) Arsenate may substitute SO_4^{2-} in the insoluble Fe hydroxy sulfates as has been suggested for jarosite by Foster et al. (1998).

(c) The arsenate may become embedded in the Fe hydroxy sulfate lattices as very small scorodite clusters. Relaxation effects may occur in small clusters, resulting in atomic distances that are decreased in comparison to the distances in the corresponding macroscopic phase.

The As K-edge results for the colloidal samples, i.e. the raw sample, the 5-μm filtrate, the 1-kD filtrate, the 1-kD retentate, in Fig. 9 and Table 5 are strikingly alike. Obviously, the arsenate is bound to the colloidal Fe

Table 5
EXAFS structural parameters for the absorber-backscatterer atomic shells obtained at the Fe K-edge and the As K-edge. The parameters are: coordination numbers N, interatomic distances R, and Debye–Waller factors σ^2

Sample	Fe K-edge				As K-edge			
	Shell	N[a]	R (Å)[b]	σ^2 (Å^{-2})	Shell	N[a]	R (Å)[b]	σ^2 (Å^{-2})
Schwertmannite $Fe_8O_8(OH)_6SO_4$	Fe–O	4.9	1.96	0.0105				
	Fe–Fe1	1.3	3.03	0.0046				
	Fe–Fe2	1.9	3.37	0.0091				
Jarosite $(H_3O,K)Fe_3(SO_4)_2(OH)_6$	Fe–O	4.0	1.99	0.0037				
	Fe–S	0.6	3.23	0.0010				
	Fe–Fe1	1.5	3.66	0.0025				
Goethite α-FeOOH	Fe–O	5.0	1.97	0.0114				
	Fe–Fe1	2.0	3.02	0.0042				
	Fe–Fe2	6.5	3.37	0.0164				
Scorodite (mineral) $FeAsO_4{\cdot}2H_2O$	Fe–O	4.5	1.97	0.0053	As–O	5.0	1.68	0.0027
	Fe–As	2.2	3.36	0.0030	As–Fe	3.7	3.34	0.0048
Bukowskyite (mineral) $Fe_2AsO_4SO_4OH{\cdot}7H_2O$	Fe–O	5.4	1.98	0.0073	As–O	5.2	1.68	0.0025
	Fe–As	0.5	3.34	0.0010	As–Fe	3.2	3.33	0.0042
ARD solution raw sample					As–O	4.3	1.69	0.0013
					As–Fe	2.2	3.28	0.0047
ARD solution (5-μm filtrate)					As–O	4.5	1.69	0.0017
					As–Fe	2.2	3.27	0.0046
ARD solution (1-kD filtrate)	Fe–O	6.0	2.00	0.0052	As–O	4.4	1.68	0.0011
	Fe–As	2.0	3.43	0.0122	As–Fe	1.9	3.26	0.0032
	Fe–Fe	0.4	3.65	0.0025				
ARD solution (1-kD retentate)	Fe–O	5.1	1.98	0.0060	As–O	4.7	1.69	0.0021
	Fe–As	0.3	3.29	0.0011	As–Fe	2.5	3.29	0.0067
	Fe–Fe	1.5	3.55	0.0118				
ARD solution, precipitate	Fe–O	5.3	1.97	0.0053	As–O	5.0	1.68	0.0022
	Fe–As	2.9	3.32	0.0104	As–Fe	4.5	3.28	0.0110
	Fe–Fe	2.2	3.62	0.0101				
0.066 M As solution					As–O	5.2	1.68	0.0025

[a] Error in coordination numbers ±25%
[b] Error in distances ±0.01 Å

hydroxy sulfate in a similar way in all these samples. It is assumed that mechanism (a) is responsible for the arsenate uptake by particles in these samples, i.e. the arsenate tetrahedron is sorbed as a corner-shared bidentate arsenate surface complex bridging the O atoms of two Fe oxyhydroxide octahedra (regardless of the degree of filtration). One might hypothesize that at least for the 1-kD ultrafiltrate there should not be much colloidal Fe hydroxy sulfate and the As-Fe contribution to the EXAFS spectrum might primarily be caused by the dissolved complexes $FeHAsO_4^+$ and $FeH_2AsO_4^{2+}$ (cf. Robins, 1987). This is, however, not really supported by the results: There is an Fe–Fe contribution to the EXAFS spectrum also in the 1-kD filtrate (Fig. 8 and Table 5) and the As is surrounded by more than one Fe atom in this filtrate (Table 5). Furthermore, the behavior of the scattered light intensity after the 1-kD filtration (cf. Section 3.3.3.) indicates that particles play a major role also in the 1-kD filtrate.

In the long-term precipitate, however, the situation has changed. Whereas the As-Fe distance is still around 3.28 Å, the coordination number increases to 4.5. This indicates a change in the coordination of As. It is attributed to an increasing influence of mechanisms (b) and/or (c) on the As uptake. A change to the incorporating uptake mechanisms (b) or (c) is also in accordance with a reduction in specific surface area by the precipitate formation process: SEM images of the long-term precipitate revealed a grain size of the μm range which is by 3 orders of magnitude higher than the size of the ultrafine colloid particles.

4. Conclusions

It has been demonstrated that the highly mineralized ARD samples from an abandoned Zn–Pb–Ag ore mine (pH 2.7, SO_4^{2-} concentration 411 mmol/l) contain a small amount (about 20 mg/l) of easily-detectable inorganic submicron particles of about 100 nm. Furthermore, there is a small amount (<5 mg/l) of organic particles of the micron size range. However, it follows from PCS,

centrifugation and filtration that these relatively large particles form only the minor colloid component. Ultrafiltration revealed that at least 15% of the Fe, 50% of the As and 80% of the Pb occur as particles of 1.3–5 nm in diameter (the geometric sizes of the 3-kD and the 100-kD filter pores, respectively). This corresponds to a colloid concentration of at least 680 mg/l Fe, 230 mg/l As and 20 mg/l Pb. In addition to this, inorganic particles between metal ion size and 1.3 nm should also be expected.

The authors tried to identify the mineralogical composition of the ultrafine particles by comparison with geochemical speciation modeling with EQ3/6, i.e. by calculating the oversaturated mineral phases which are the potential colloid-forming compounds. The experimetal findings for the colloidal fraction of Pb coincide with the model prediction of nearly quantitative precipitation of anglesite ($PbSO_4$). Also the detected concentration of Fe colloids is not in contradiction to the model output. Here, however, several mineral phases are possible, depending on the solubility data set applied for schwertmannite, ferrihydrite, and various jarosite phases. Finally, the large fraction of colloidal As must be interpreted as, probably metastable, scorodite according to the EQ3/6 calculations. Another hypothesis is that of a substantial adsorption of As onto the Fe hydroxy sulfates. A literature survey was started to compile a thermodynamic data set for surface complexation modeling, which may deliver further insight. The EQ3/6 calculations proved to be a valuable tool to select reference model compounds for EXAFS measurements.

According to the EXAFS measurements, the most probable mineralogical composition of the colloid particles is a mixture of hydronium jarosite and schwertmannite. The coexistence of schwertmannite and jarosite in the particles suggests that schwertmannite is less soluble than postulated by Bigham et al. (1996) supporting the findings by Yu et al. (1999). It seems that the composition of the colloidal particles and the composition of the long-term precipitate are quite similar. Thus the colloid particles can be regarded as an intermediate of the precipitate formation process. Only the degree of crystallization increases when particles are transformed into the precipitate. The present results suggest that the arsenate is bound to the colloid particles by surface complexation (formation of a bidentate binuclear inner-sphere complex). However, the transformation of the colloidal material into the more aggregated long-term precipitate seems to result in a change of the arsenate binding in this material. Obviously, the incorporation of the arsenate into the interior of the Fe hydroxy sulfate crystal structures is more pronounced in the precipitate. The mechanisms of this incorporation could be the substitution of arsenate for sulfate in the jarosite structure and/or the formation of very small scorodite clusters as occlusions within jarosite.

Acknowledgements

This paper represents publication no. 161 of the Priority Program 546 'Geochemical processes with long-term effects in anthropogenically-affected seepage and groundwater'. Financial support was provided by *Deutsche Forschungsgemeinschaft*. We thank C. Fröhlich for assistance in the chemical laboratory work, E. Christalle for the SEM and EDX investigations, W. Wiesener and her group for the ICP-MS and AAS analyses and A. Scholz for the XRD investigations. We also thank T. Arnold for providing us with the schwertmannite sample and K. Flemming, J. Raff and M. Merroun for supplying the jarosite. Furthermore, the help of A. Rossberg, and H. Funke during the EXAFS measurements at ROBL is gratefully acknowledged.

References

Arnold, T., Bernhard, G., Nitsche, H., 1999. Report FZR-247, Annual Report of Institute of Radiochemistry of the year 1998, Forschungszentrum Rossendorf, p. 17.

Balistrieri, L.S., Box, E.S., Bookstrom, A.A., Ikramuddin, M., 1999. Assessing the influence of reacting pyrite and carbonate minerals on the geochemistry of drainage in the Coer d'Alene mining district. Environ. Sci. Technol. 33, 3347–3353.

Bayer, M., 1998. Die Himmelfahrt Fundgrube. Ein Führer durch das Lehr- und Besucherbergwerk der TU Berakademie Freiberg. TU Bergakademie Freiberg, Freiberg University of Mining and Technology.

Bigham, J.M., Schwertmann, U., Traina, S.J., Winland, R.L., Wolf, M., 1996. Schwertmannite and the chemical modeling of iron in acid sulfate waters. Geochim. Cosmochim. Acta 60, 2111–2121.

Buffle, J., Leppard, G.G., 1995. Characterization of aquatic colloids and macromolecules. 2. Key role of physical structures on analytical results. Environ. Sci. Technol. 29, 2176–2184.

Byrne, R.H., Luo, Y.-R., 2000. Direct observations of nonintegral hydrous ferric oxide solubility products: $K^*_{SO} = [Fe^{3+}][H^+]^{-2.86}$. Geochim. Cosmochim. Acta 64, 1873–1877.

Charlet, L., Manceau, A., 1993. Structure, formation, and reactivity of hydrous oxide particles: insights from X-ray absorption spectroscopy. In: Buffle, J., Van Leeuven, H.P. (Eds.), Environmental Particles. IUPAC Series on Environmental Analytical and Physical Chemistry, Vol. 2. Lewis Publishers, Boca Raton, pp. 117–164.

Cornell, R.M., Schwertmann, U., 1996. The Iron Oxides. Structure, Properties, Reactions, Occurrence and Uses. VCH, Weinheim.

Davis, A., Ruby, M.V., Goad, P., Eberle, S., Chryssoulis, S., 1997. Mass balance on surface-bound, mineralogic, and total lead concentrations as related to industrial aggregate bioaccessibility. Environ. Sci. Technol. 31, 37–44.

DIN 38 406, 1983. Deutsche Einheitsverfahren zur Wasser-, Abwasser- und Schlammuntersuchung. Kationen (Gruppe E). Bestimmung von Eisen.

Fendorf, S., Eick, M.J., Grossl, P., Sparks, D.L., 1997. Arsenate and chromate retention mechanisms on goethite. 1. Surface structure. Environ. Sci. Technol. 31, 315–320.

Ford Jr, N.C., 1985. Light scattering apparatus. In: Pecora, R. (Ed.), Dynamic Light Scattering. Plenum Press, New York, pp. 7–58.

Foster, A.L., Brown Jr, G.E., Tingle, T.N., Parks, G.A., 1998. Quantitative arsenic speciation in mine tailings using X-ray absorption spectroscopy. Amer. Mineralogist 83, 553–568.

Fuller, C.C., Davis, J.A., Waychunas, G.A., 1993. Surface chemistry of ferrihydrite: Part 2. Kinetics of arsenate adsorption and coprecipitation. Geochim. Cosmochim. Acta 57, 2271–2282.

Geller, W., Kappler, H., Salomons, W. (Eds.), 1996. Acidic Mining Lakes. Springer, Berlin.

George, G.N., Pickering, I.J., 1995. EXAFSPAK, A suite of computer programs for analysis of X-ray absorption spectra. Stanford Synchrotron Radiation Laboratory, Stanford, USA.

Grabowski, E.E., Morrison, I.D., 1983. Particle size distribution from analysis of quasi-elastic light-scattering data. In: Dahneke, B.E. (Ed.), Measurement of Suspended Particles by Quasi-Elastic Light Scattering. Wiley-Interscience, New York, pp. 199–236.

Haubrich, F., Baacke, D., Winkler, C., 1999. Sulfidverwitterung in aufgefahrenen Erzgängen—ein Feld komplexer geochemischer Forschung. GUG-Schriftenreihe Geowissenschaften und Umwelt, TU Bergakademie Freiberg.

Iler, R.K., 1979. The Chemistry of Silica. John Wiley & Sons, New York.

Koningsberger, D.E., Prins, R., 1988. X-ray Absorption. Principles, Applications, Techniques for EXAFS, SEXAFS, and XANES. Wiley-Intersience, New York.

Lindberg, R.D., Runnells, D.D., 1984. Ground water redox reactions: an analysis of equilibrium state applied to Eh measurements and geochaemical modeling. Science 225, 925–927.

Magini, M., 1977. Structural relationships between colloidal solutions and hydroxide gels of iron(III) nitrate. J. anorg. nucl. Chem. 39, 409–412.

Manceau, A., 1995. The mechanism of anion adsorption on iron oxides: evidence for the bonding of arsenate tetrahedra on free $Fe(O,OH)_6$ edges. Geochim. Cosmochim. Acta 59, 3647–3653.

Manceau, A., Charlet, L., Boisset, M.C., Didier, B., Spadini, L., 1992. Sorption and speciation of heavy metals on hydrous Fe and Mn oxides. From microscopic to macroscopic. Appl. Clay Sci. 7, 201–223.

Matz, W., Schell, N., Bernhard, G., Prokert, F., Reich, T., Claußner, J., Oehme, W., Schlenk, R., Dienel, S., Funke, H., Eichhorn, F., Betzl, M., Pröhl, D., Strauch, U., Hüttig, G., Krug, H., Neumann, W., Brendler, V., Reichel, P., Denecke, M.A., Nitsche, H., 1999. ROBL - a CRG beamline for radiochemistry and material research at the ESFR. J. Synchrotron Rad. 6, 1076–1085.

Moll, H., Zänker, H., Richter, W., Brendler, V., Reich, T., Hennig, C., Roβberg, A., Funke, H., Kluge, A., 2000. XAS Study of acid rock drainage samples from an abandoned Zn-Pb-Ag mine at Freiberg, Germany. 2nd Euroconference and NEA Workshop on Speciation, Techniques, and Facilities for Radioactive Materials at Synchrotron Light Sources. Actinide-XAS-2000. 10–12 September, Grenoble, France.

Nordstrom, D.K., Alpers, C.N., Ptacek, C.J., Blowes, D.W., 2000. Negative pH and extremely acidic mine waters from iron mountain, California. Environ. Sci. Technol. 34, 254–258.

Paulson, J.A., Balistrieri, L., 1999. Modeling removal of Cd, Cu, Pb, and Zn in acidic groundwater during neutralization by ambient surface waters and groundwaters. Environ. Sci. Technol. 33, 3850–3856.

Pleβow, A., Heinrichs, H., 2000. Speciation of trace elements in acidic pore waters from waste rock dumps by ultrafiltration and ion exchange combined with ICPMS and ICPOES. Aqu. Geochem. 6, 347–366.

Powder Diffraction File, 1991. International Center of Diffraction Data, Newton Square, USA, Diffraction Data Card No. 36-427.

Provencher, W., 1982. A constrained regularization method for inverting data presented by linear algebraic or integral equations. Comput. Phys. Commun. 27, 213–227.

Robins, R.G., 1987. Solubility and stability of scorodite, $FeAsO_4{\cdot}2H_2O$: discussion. Am. Mineral. 72, 842–844.

Schurtenberger, P., Newman, M.E., 1993. Characterization of biological and environmental particles using static and dynamic light scattering. In: Buffle, J., Van Leeuven, H.P. (Eds.), Environmental Particles. IUPAC Series on Environmental Analytical and Physical Chemistry, Vol. 2. Lewis Publishers, Boca Raton, pp. 37–116.

Schwertmann, U., Friedl, J., Stanjek, H., 1999. From Fe(III) ions to ferrihydrite and then to hematite. J. Colloid Interface Sci. 209, 215–223.

Stock, R.S., Ray, W.H., 1985. Interpretation of photon correlation spectroscopy data: a comparison of analysis methods. J. Polym. Sci.: Polym. Phys. Ed. 23, 1393–1447.

Wang, W.-X., Guo, L., 2000. Influences of natural colloids on metal bioavailability to two marine bivalves. Environ. Sci. Technol. 34, 4571–4576.

Waychunas, G.A., Davis, J.A., Fuller, C.C., 1995. Geometry of sorbed arsenate on ferrihydrite and crystalline FeOOH: reevaluation of EXAFS results and topological factors in predicting sorbate geometry, and evidence for monodentate complexes. Geochim. Cosmochim. Acta 59, 3655–3661.

Waychunas, G.A., Fuller, C.C., Rea, B.A., Davis, J.A., 1996. Wide angle X-ray scattering (WAXS) study of "two-line" ferrihydrite structure: effect of arsenate sorption and counterion variation and comparison with EXAFS results. Geochim. Cosmochim. Acta 60, 1765–1781.

Waychunas, G.A., Rea, B.A., Fuller, C.C., Davis, J.A., 1993. Surface chemistry of ferrihydrite: part 1. EXAFS studies of geometry of coprecipitated and adsorbed arsenate. Geochim. Cosmochim. Acta 57, 2251–2269.

Weiner, B.R., 1984. Particle sizing using photon correlation spectroscopy. In: Barth, H.G. (Ed.), Modern Methods of Particle Sizing. John Wiley & Sons, New York.

Winland, R.L., Traina, S.J., Bigham, J.M., 1991. Chemical composition of ochreous precipitates from Ohio coal mine drainage. J. Environ. Qual. 20, 452–460.

Wolery, T.J., 1992. A software package for the geochemical modeling of aqueous systems. Report URCL-MA-110662. Part I. Lawrence Livermore National Laboratory. Livermore.

Yu, J.-Y., Heo, B., Choi, I.-K., Cho, J.-P., Chang, H.-W., 1999. Apparent solubilities of schwertmannite and ferrihydrite in natural stream waters polluted by mine drainage. Geochim. Cosmochim. Acta 63, 3407–3416.

Zabinsky, S.I., Rehr, J.J., Ankudinov, A., Albers, R.C., Eller, M.J., 1995. Multiple-scattering calculations of X-ray-absorption spectra. Phys. Rev. B 52, 2995–3008.

Zänker, H., Richter, W., Brendler, V., Nitsche, H., 2000. Colloid-borne uranium and other heavy metals in the water of a mine drainage gallery. Radiochim. Acta 88, 619–624.